第 44 卷 第 10 期/2024 年 5 月/光学学报 特邀论文

光学学报

基于全介质一维光子晶体的平面拓扑微分器(特邀)

刘洋, 黄明川, 陈钱坤, 张斗国*

中国科学技术大学物理学院光学与光学工程系先进激光技术安徽省实验室, 安徽 合肥 230026

摘要 提出一种拓扑荷数为2的全介质一维光子晶体拓扑微分运算器件。通过优化设计光子晶体的透射率与入射角度的依赖关系以及出/入射光的偏振状态,该拓扑器件可以对入射光场进行各向同性的二维二阶光学微分运算,进而实现图像边缘增强成像和图像边缘信息高效提取。该平面型拓扑微分运算器件具有轻量化、高通量、高速度、易于大规模集成、低成本制备等特点,在光学计算、光学成像与传感等领域具有潜在的应用价值。

关键词 物理光学; 光学拓扑微分运算; 边缘检测; 全介质一维光子晶体; 光学成像与传感。

中图分类号 O436 **文献标志码** A **DOI**: 10.3788/AOS231951

1 引 言

光计算具有大通量、高处理速度以及低损耗的特性,在机器学习和高性能计算领域有巨大的应用价值[1-6]。传统的光计算是在傅里叶空间中利用光学元件进行光场调控来实现的,但是这些构架会占用大量空间[7]。得益于微纳加工技术的发展,紧实、高效的超表面和超构材料器件取代了传统的大体积光学元件,这一进展重新引起人们对于光计算的兴趣。空间微分运算是光计算的一个重要组成部分,其作为一种图像处理技术可以被用来实现图像边缘检测。近年来,许多用于空间微分运算的微纳光学元件被提出和实现,如一维微分运算器件[8-12]和非各向同性二维微分运算器件[13-15]。基于拓扑性质的微分器件可以实现各向同性的二维微分运算,但目前实验上实现的该类微分器件工作于反射模式[16],不利于集成至光学成像与计算系统。

本文通过实验实现了一种基于全介质一维光子晶体芯片的平面透射式光学微分器件,该器件可以实现二维二阶光学空间微分运算[17]。该一维光子晶体可以作为光学芯片插入传统的商业显微系统,对入射光场进行动量空间光场调制。利用该光学芯片的非局域特性[18-20],通过精确调控其透射率与入射角度的依赖关系来实现微分运算所需的光学传递函数,同时控制出射光和入射光的偏振态为正交圆偏振状态以实现拓扑微分运算。该全介质的一维光子晶体光学芯片可以通过标准的化学气相沉积技术大规模制备[13, 21]。本文利用标准分辨率靶样品对该光学芯片的微分运算功能进行实验验证,并成功将该微分运算器件应用到生物样品的边缘增强成像。

2 基本原理

根据傅里叶光学原理[7],光学芯片调制前的入射场 $\boldsymbol{E}_{\mathrm{in}}(x,y)$ 以及调制后的出射场 $\boldsymbol{E}_{\mathrm{out}}(x,y)$ 可以在频谱空间中被展开为面内横纵向波矢量 k_x 和 k_y 的函数:

$$\boldsymbol{E}_{\mathrm{in}}(x,y)=\boldsymbol{e}_{\mathrm{in}}\iint A(k_x,k_y)\exp(\mathrm{i}k_x x+\mathrm{i}k_y y)\mathrm{d}k_x\mathrm{d}k_y, \tag{1}$$

$$\boldsymbol{E}_{\mathrm{out}}(x,y)=\boldsymbol{e}_{\mathrm{out}}\iint t(k_x,k_y)A(k_x,k_y)\times \exp(\mathrm{i}k_x x+\mathrm{i}k_y y)\mathrm{d}k_x\mathrm{d}k_y, \tag{2}$$

式中:$\boldsymbol{e}_{\mathrm{in(out)}}$ 为入射(出射)光的偏振状态;$A(k_x,k_y)$ 为电磁场的振幅;$t(k_x,k_y)$ 为由光学芯片引入的光学传递函数,其表征光学芯片对入射场的调制效果。当光学传递函数满足 $t(k_x,k_y)\propto k_{\mathrm{r}}^{n}\left(k_{\mathrm{r}}=\sqrt{k_x^2+k_y^2}\right)$ 时,出射的电磁场相对于入射的电磁场进行了二维 n 阶微分运算。值得注意的是,该处的微分运算是沿着入射光在样品平面投影的方向进行的。

光学传递函数 $t(k_x,k_y)$ 与入射场和出射场有关,可以表示为

$$t(k_x,k_y)=\boldsymbol{e}_{\mathrm{out}}^{*}\boldsymbol{M}^{-1}\boldsymbol{T}(k_x,k_y)\boldsymbol{M}\boldsymbol{e}_{\mathrm{in}}, \tag{3}$$

式中:$\boldsymbol{T}(k_x,k_y)=\begin{bmatrix} t_{\mathrm{S}}(k_x,k_y) & 0 \\ 0 & t_{\mathrm{P}}(k_x,k_y)\end{bmatrix}$ 为以S和P偏

收稿日期: 2023-12-19; **修回日期**: 2024-01-25; **录用日期**: 2024-01-29; **网络首发日期**: 2024-02-20

基金项目: 国家自然科学基金(12134013, 62127818)、国家重点研发计划(2021YFA1400700)、安徽省重点研究与开发计划项目(202104a05020010)、中央高校基本科研业务费专项(WK2340000109)

通信作者: *dgzhang@ustc.edu.cn

振方向为基的光学芯片透射系数矩阵；$t_S(k_x,k_y)$和$t_P(k_x,k_y)$分别为S偏振光和P偏振光的菲涅耳透射系数。矩阵$\boldsymbol{M}$为从以x和y为基到以S和P为基的变换矩阵，即

$$\boldsymbol{M}=\begin{bmatrix}-\cos\varphi & \sin\varphi\\ \sin\left[\varphi\left(1+\frac{\theta^2}{2}\right)\right] & \cos\left[\varphi\left(1+\frac{\theta^2}{2}\right)\right]\end{bmatrix}。\tag{4}$$

在小角度范围内$\theta=\arcsin\left(\frac{k_r}{k_0}\right)\approx\frac{k_r}{k_0}$，$\varphi=\arctan\left(\frac{k_y}{k_x}\right)$，$k_0$为电磁场在真空中的波数。为了满足二阶微分的要求，菲涅耳透射系数需要被泰勒展开至二次项，且其高阶项忽略不计，即$t_{S(P)}(k_x,k_y)=t_0+C_{S(P)}\theta^2$，其中$t_0$为正入射光的透射率，$C_{S(P)}$为二次项常系数。

联立式(3)和式(4)可以得到光学传递函数：

$$t(k_x,k_y)=e_{out}^{x*}e_{in}^{x}\theta^2\left(C_S\sin^2\varphi+C_P\cos^2\varphi\right)+e_{out}^{x*}e_{in}^{y}\theta^2\left[\frac{\sin(2\varphi)}{2}(C_P-C_S)\right]+e_{out}^{y*}e_{in}^{x}\theta^2\left[\frac{\sin(2\varphi)}{2}(C_P-C_S)\right]+$$
$$e_{out}^{y*}e_{in}^{y}\theta^2\left(C_P\sin^2\varphi+C_S\cos^2\varphi\right)。\tag{5}$$

采用线偏振光入射的非拓扑微分运算器件无法实现各向同性的微分运算[13,22]，本文通过引入拓扑荷使二阶微分运算具有旋转对称性，从而实现各向同性的微分运算。将入射光的偏振状态设置为左旋圆偏振态$\boldsymbol{e}_{in}=\frac{1}{\sqrt{2}}\begin{bmatrix}1\\ \mathrm{i}\end{bmatrix}$，出射光的偏振状态设置为右旋圆偏振态$\boldsymbol{e}_{out}=\frac{1}{\sqrt{2}}\begin{bmatrix}1\\ -\mathrm{i}\end{bmatrix}$。通过自旋-轨道转换效应[23-26]，经过样品的散射自旋角动量转化为$l=2$的轨道角动量，同时正交偏振态也抑制了光学传递函数的正入射透射率($t_0=0$)。最终的光学传递函数具有如下形式：

$$t(k_x,k_y)=\theta^2\exp(\mathrm{i}2\varphi)\frac{(C_P-C_S)}{2}\propto(k_x+\mathrm{i}k_y)^2。\tag{6}$$

由式(6)可知，光学传递函数存在一个二阶拓扑荷。为了验证拓扑微分运算的旋转对称性，令$\boldsymbol{H}(\boldsymbol{k})=\boldsymbol{M}^{-1}\boldsymbol{T}(\boldsymbol{k})\boldsymbol{M}$，旋转算符$\hat{R}$可对面内矢量旋转$\phi$角，则有

$$t[R(\boldsymbol{k})]=\boldsymbol{e}_{out}^{*}\boldsymbol{H}[R(\boldsymbol{k})]\boldsymbol{e}_{in}=\boldsymbol{e}_{out}^{*}\hat{R}\boldsymbol{H}(\boldsymbol{k})\hat{R}^{-1}\boldsymbol{e}_{in}=$$
$$\exp(\mathrm{i}2\phi)\boldsymbol{e}_{out}^{*}\boldsymbol{H}(\boldsymbol{k})\boldsymbol{e}_{in}=\exp(\mathrm{i}2\phi)t(\boldsymbol{k})。\tag{7}$$

由式(7)可知，上述体系具有旋转对称性，带有二阶拓扑荷的光学芯片可以实现二维二阶各向同性的空间微分运算。

3　分析与讨论

3.1　光学芯片的设计与表征

为了实现二维二阶空间微分运算，光学芯片需要满足的条件是：正入射光场的透射率趋近于0，且对S和P偏振光场的透射率正比于面内波矢的二次方[27]，即$t_{S(P)}(k_x,k_y)\propto k_r^2$。本文采用全介质一维光子晶体来实现这一光学空间微分运算过程。为了增加禁带深度以使得正入射透射率趋近于0，采用高堆叠层数的一维光子晶体，该光子晶体由20对(40层)高折射率介质(Si_3N_4)和低折射率介质(SiO_2)层纵向交替排布构成，如图1(a)、(b)所示。这两种材料在可见光波段具有较高的透射率，可被运用于透射式显微系统中，其折射率分别为2.53和1.46。图1(c)所示为利用转移矩阵法[28-29]计算得到的该一维光子晶体的透射率分布，通过在计算过程中调节两种材料的层厚，使其在入射波长为635 nm处的透射率对面内波矢呈二次方的依赖关系，此时这两种材料的层厚分别为59 nm和72 nm。同时，由于高堆叠层数引入高禁带深度，该光子晶体对波长为635 nm的正入射光的透射率趋近于0。

为了验证该光学芯片的微分运算性能，利用等离子增强化学气相沉积技术制备该全介质一维光子晶体芯片。在实验过程中，左旋圆偏振光入射至该光学芯片，经过样品衍射和光学芯片调制的出射光的右旋圆偏振成分被显微系统成像到探测器。图1(d)所示为该光学芯片的后焦面图像，该图像由被收集的右旋圆偏振光在频谱空间中成像得到，因此其动量空间位置(k_x,k_y)对应于光场的传播方向。后焦面中心为暗斑，表明该光学芯片对正入射光场的透射率趋近于0[30]。为了检验其各向同性的微分运算性能，沿着图1(d)中白色虚线绘制了光学传递函数强度截面，如图1(e)所示。不同方位角度的光学传递函数强度截面表示沿不同方向的微分运算，其均可被二次方曲线很好地拟合。这表明该光学芯片对入射光的透射率与面内波矢呈二次方关系，且该依赖关系不随方位角改变，表明该光学芯片可以实现各向同性的二维二阶微分运算。

本实验采用干涉测量的方法来表征上述微分运算体系的拓扑荷数[31]。如图2(a)所示，检测光路分为两路：一路依次加入起偏器1(P1)、四分之一波片1(QWP1)、光学芯片、四分之一波片2(QWP2)和检偏器2(P2)，以产生二阶拓扑荷，经过该路的调制光场以平面波的形式被探测器接收；另一路为参考光，通过调节偏振片P3和P4的夹角来达到与调制光相近的振幅强度，该路光波以球面波的形式被探测器接收。图2(b)为调制光和参考光干涉得到的涡旋光场干涉图样，该图样由两条涡旋条纹组成，这表明经过调制的光场携带了二阶拓扑荷。

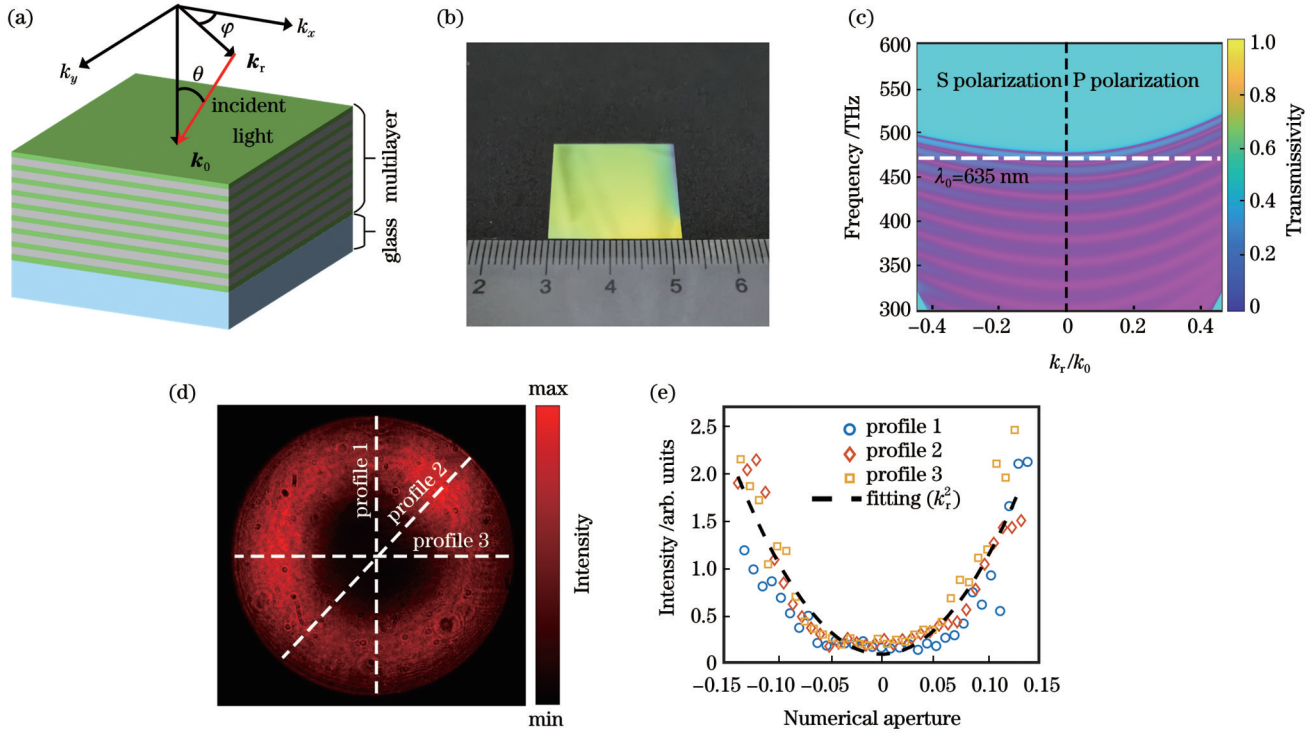

图 1 全介质一维光子晶体芯片的设计与表征。(a)光子晶体芯片结构示意图;(b)光子晶体芯片实物照片;(c)光子晶体芯片的透射谱;(d)光子晶体芯片的后焦面;(e)沿着图 1(d)中相应白色虚线提取得到的光学传递函数强度截面及二次方拟合曲线

Fig. 1 Design and characterization of an all-dielectric one-dimensional photonic crystal (1DPC) chip. (a) Diagram of 1DPC chip structure; (b) photograph of the fabricated planar 1DPC chip; (c) transmission spectrum of 1DPC chip; (d) back focal plane image of 1DPC chip; (e) intensity profiles of optical transfer functions along the dashed lines in Fig. 1(d) and the corresponding quadratic fitting curve

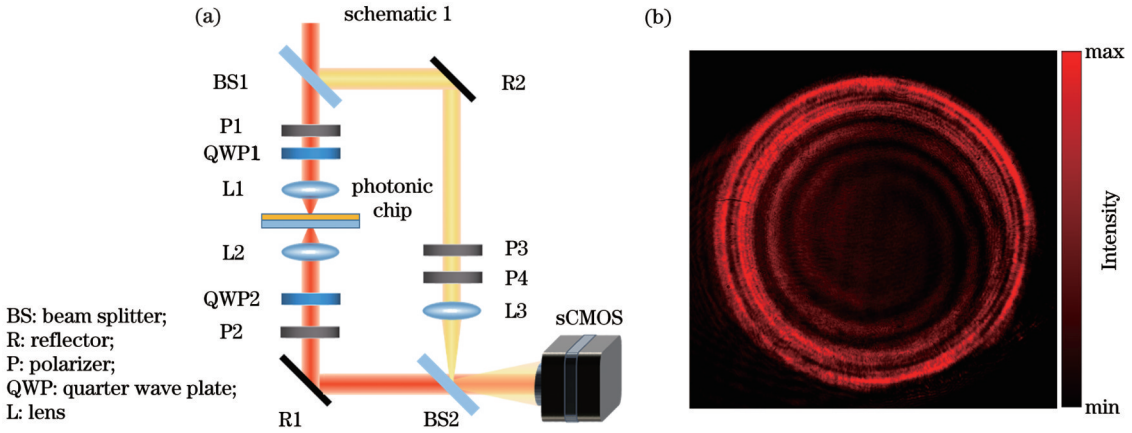

图 2 拓扑微分器的表征。(a)用于检测拓扑荷数的干涉测量光路;(b)涡旋光场干涉图样

Fig. 2 Characterization of topological differentiator. (a) Schematic of interferometric measurement lightpath for detecting topological charges; (b) interference pattern of vortex light field

3.2 光学芯片的空间微分运算效果

该光学芯片的优势之一是可以被整合到传统显微成像系统中,对携带样品信息的光场进行微分运算处理。在本实验中,制备好的光学芯片被直接插入到透射式显微镜中,并位于待测样品的底部,如图 3(a)所示。左旋圆偏振态的入射光会聚在位于光学芯片上方的振幅阶跃型样品(1951 USAF 分辨率测试靶),为样品提供大角度范围的照明。被光学芯片调制的光场经过 QWP2 和 P2 的偏振选择,其右旋圆偏振分量被提取出来进行成像[图 3(a)]。图 3(b)所示为分辨率测试靶在明场显微镜下的像,其中不透光区域为图像背景,透光区域构成了数字和刻线图样。值得注意的是,当对该振幅阶跃型样品的边缘进行 n 阶微分运算时,像面中边缘所在位置会出现 n 个峰[13]。图 3(c)为分辨率测试靶在微分运算体系下的像,插图中图样边缘处出现两个峰,这表明该图像相对于

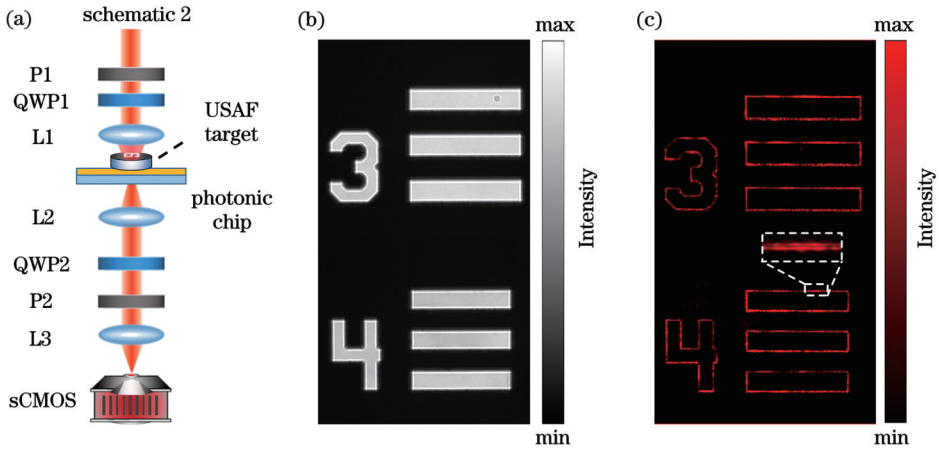

图 3 微分运算器件对前焦面成像的调制效果。(a)前焦面成像光路;(b) 1951 USAF 分辨率靶明场像;(c) 1951 USAF 分辨率靶微分成像,其中插图为边缘的放大图像

Fig. 3 Modulation effect of differential device on the front focal plane. (a) Schematic of experimental setup for front focal plane imaging; (b) bright field image of the 1951 USAF resolution chart; (c) differential image of the 1951 USAF resolution chart, the inserted image is the enlarged image of an edge

明场图像进行了二维二阶微分运算。微分图像中的数字由多角度刻线拼凑而成,其边缘均被清晰地提取出来,表明该器件可以实现各向同性的图像边缘信息提取。

与此同时,携带生物样品(如洋葱皮细胞)信息的光场也可以在该体系下进行微分运算操作。由于生物细胞为弱散射样品[32-34],这些样品对入射光场振幅的调制效应较弱,在传统明场显微镜下无法观测到清晰轮廓[图 4(a)]。将该洋葱表皮细胞放置到拓扑微分运算体系(制备的全介质一维光子晶体器件放在洋葱皮细胞样品的下方),其边缘特征被清晰地提取出来并且成像对比度增大,如图 4(b)所示。实验结果表明,该一维光子晶体器件在生物样品检测领域具有潜在应用价值。

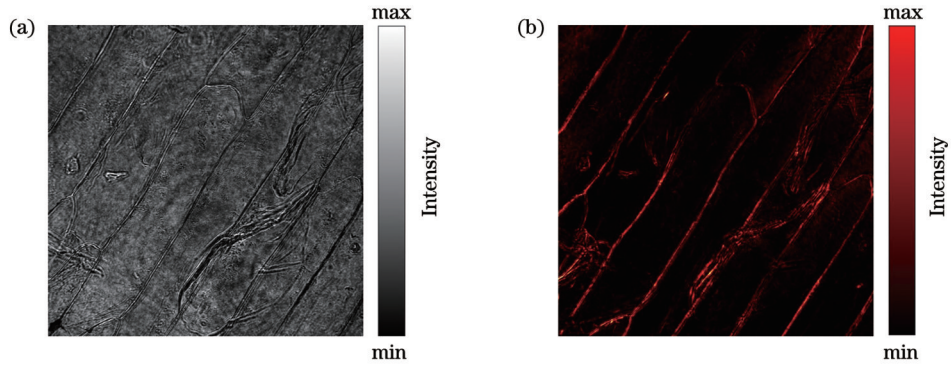

图 4 洋葱表皮细胞的明场图像和微分运算图像。(a)明场图像;(b)微分运算图像

Fig. 4 Bright field image and differential image of onion epidermal cells. (a) Bright field image; (b) differential image

4 结 论

设计和加工了一种工作在透射模式下的二维二阶拓扑微分光学芯片。该光学芯片由全介质一维光子晶体组成。通过调节光子晶体的结构参数,可以获得二阶微分运算所需要的光学传递函数。当入射光和出射光的偏振状态分别为正交的左旋圆偏振态和右旋圆偏振态时,光学传递函数中会产生一个二阶的拓扑荷,从而实现各向同性的二维微分运算。利用制备所得的光学芯片,展示了其对携带有分辨率靶和生物样品信息的入射光场的微分运算效果。得益于成熟的全介质一维光子晶体样品制备技术,所设计的光学芯片可以被大规模、低成本地制备。该拓扑微分光学芯片具有大通量、高速度、各向同性的运算性能,在图像处理、机器视觉和显微成像与传感等领域有潜在应用价值。

参 考 文 献

[1] Silva A, Monticone F, Castaldi G, et al. Performing mathematical operations with metamaterials[J]. Science, 2014, 343(6167): 160-163.

[2] Sihvola A. Enabling optical analog computing with metamaterials [J]. Science, 2014, 343(6167): 144-145.

[3] Solli D R, Jalali B. Analog optical computing[J]. Nature

Photonics, 2015, 9: 704-706.

[4] 刘世凯, 周志远, 史保森. 光学图像边缘检测技术研究进展[J]. 激光与光电子学进展, 2021, 58(10): 1011014.
Liu S K, Zhou Z Y, Shi B S. Progress on optical image edge detection[J]. Laser & Optoelectronics Progress, 2021, 58(10): 1011014.

[5] 陈蓓, 张肇阳, 戴庭舸, 等. 光学神经网络及其应用[J]. 激光与光电子学进展, 2023, 60(6): 0600001.
Chen B, Zhang Z Y, Dai T G, et al. Photonic neural networks and its applications[J]. Laser & Optoelectronics Progress, 2023, 60(6): 0600001.

[6] 符庭钊, 孙润, 黄禹尧, 等. 片上集成光学神经网络综述(特邀)[J]. 中国激光, 2024, 51(1): 0119002.
Fu T Z, Sun R, Huang Y Y, et al. Review of on-chip integrated optical neural networks (Invited)[J]. Chinese Journal of Lasers, 2024, 51(1): 0119002.

[7] Goodman J W. Introduction to Fourier optics[M]. 3rd ed. Englewood: Roberts & Co., 2005.

[8] Wesemann L, Rickett J, Song J C, et al. Nanophotonics enhanced coverslip for phase imaging in biology[J]. Light: Science & Applications, 2021, 10(1): 98.

[9] Zhu T F, Lou Y J, Zhou Y H, et al. Generalized spatial differentiation from the spin Hall effect of light and its application in image processing of edge detection[J]. Physical Review Applied, 2019, 11(3): 034043.

[10] Zhou J X, Qian H L, Chen C F, et al. Optical edge detection based on high-efficiency dielectric metasurface[J]. Proceedings of the National Academy of Sciences of the United States of America, 2019, 116(23): 11137-11140.

[11] Davis T J, Eftekhari F, Gómez D E, et al. Metasurfaces with asymmetric optical transfer functions for optical signal processing [J]. Physical Review Letters, 2019, 123(1): 013901.

[12] Kwon H, Arbabi E, Kamali S M, et al. Single-shot quantitative phase gradient microscopy using a system of multifunctional metasurfaces[J]. Nature Photonics, 2020, 14: 109-114.

[13] Liu Y, Huang M C, Chen Q K, et al. Single planar photonic chip with tailored angular transmission for multiple-order analog spatial differentiator[J]. Nature Communications, 2022, 13(1): 7944.

[14] Zhou Y, Zheng H Y, Kravchenko I I, et al. Flat optics for image differentiation[J]. Nature Photonics, 2020, 14: 316-323.

[15] Kwon H, Cordaro A, Sounas D, et al. Dual-polarization analog 2D image processing with nonlocal metasurfaces[J]. ACS Photonics, 2020, 7(7): 1799-1805.

[16] Zhu T F, Guo C, Huang J Y, et al. Topological optical differentiator[J]. Nature Communications, 2021, 12(1): 680.

[17] Long O Y, Guo C, Wang H W, et al. Isotropic topological second-order spatial differentiator operating in transmission mode [J]. Optics Letters, 2021, 46(13): 3247-3250.

[18] Jin C Q, Yang Y M. Transmissive nonlocal multilayer thin film optical filter for image differentiation[J]. Nanophotonics, 2021, 10(13): 3519-3525.

[19] Goh H, Alù A. Nonlocal scatterer for compact wave-based analog computing[J]. Physical Review Letters, 2022, 128(7): 073201.

[20] Kwon H, Sounas D, Cordaro A, et al. Nonlocal metasurfaces for optical signal processing[J]. Physical Review Letters, 2018, 121(17): 173004.

[21] Kuai Y, Chen J X, Fan Z T, et al. Planar photonic chips with tailored angular transmission for high-contrast-imaging devices [J]. Nature Communications, 2021, 12: 6835.

[22] Zhu T F, Zhou Y H, Lou Y J, et al. Plasmonic computing of spatial differentiation[J]. Nature Communications, 2017, 8: 15391.

[23] Bliokh K Y, Ostrovskaya E A, Alonso M A, et al. Spin-to-orbital angular momentum conversion in focusing, scattering, and imaging systems[J]. Optics Express, 2011, 19(27): 26132-26149.

[24] Rodríguez-Herrera O G, Lara D, Bliokh K Y, et al. Optical nanoprobing via spin-orbit interaction of light[J]. Physical Review Letters, 2010, 104(25): 253601.

[25] Fang Y Q, Han M, Ge P P, et al. Photoelectronic mapping of the spin-orbit interaction of intense light fields[J]. Nature Photonics, 2021, 15: 115-120.

[26] Dogariu A, Schwartz C. Conservation of angular momentum of light in single scattering[J]. Optics Express, 2006, 14(18): 8425-8433.

[27] Guo C, Xiao M, Minkov M, et al. Photonic crystal slab Laplace operator for image differentiation[J]. Optica, 2018, 5(3): 251-256.

[28] Yeh P, Yariv A, Hong C S. Electromagnetic propagation in periodic stratified media. I. General theory[J]. Journal of the Optical Society of America A, 1977, 67(4): 423-438.

[29] Yariv A, Yeh P. Electromagnetic propagation in periodic stratified media. II. Birefringence, phase matching, and X-ray lasers[J]. Journal of the Optical Society of America A, 1977, 67 (4): 438-48.

[30] Zhang D G, Yuan X C, Bouhelier A, et al. Active control of surface plasmon polaritons by optical isomerization of an azobenzene polymer film[J]. Applied Physics Letters, 2009, 95 (10): 101102.

[31] Yao A M, Padgett M J. Orbital angular momentum: origins, behavior and applications[J]. Advances in Optics and Photonics, 2011, 3(2): 161-204.

[32] Zhou J X, Qian H L, Zhao J X, et al. Two-dimensional optical spatial differentiation and high-contrast imaging[J]. National Science Review, 2021, 8(6): nwaa176.

[33] Zhu T F, Huang J Y, Ruan Z C. Optical phase mining by adjustable spatial differentiator[J]. Advanced Photonics, 2020, 2 (1): 016001.

[34] Park Y, Depeursinge C, Popescu G. Quantitative phase imaging in biomedicine[J]. Nature Photonics, 2018, 12: 578-589.

Planar Topological Differentiator Based on All-Dielectric One-Dimensional Photonic Crystal (Invited)

Liu Yang, Huang Mingchun, Chen Qiankun, Zhang Douguo*

Advanced Laser Technology Laboratory of Anhui Province, Department of Optics and Optical Engineering, School of Physical Sciences, University of Science and Technology of China, Hefei 230026, *Anhui, China*

Abstract

Objective Edge detection technology based on optical analog differentiation is widely employed in fields such as microscopic imaging, data processing, and machine vision. In recent years, with the development of nanofabrication technology, various optical analog differentiators utilizing metasurfaces and metamaterials have been invented, which highly reduces the space required for optical imaging systems. We plan to propose a topological differentiator with a topological charge of 2 based on an all-dielectric one-dimensional photonic crystal (1DPC). By properly designing the bandgap structure of the 1DPC and the polarization state of input and output light fields, this topological device can perform isotropic two-dimensional second-order differential operations on the input optical field, leading to edge enhancement imaging and highly efficient edge information extraction.

Methods The photonic chip is fabricated via PECVD (Oxford System 100, UK) of SiO_2 and Si_3N_4 layers on a standard microscope cover slip. All experiments are performed using a modified upright optical microscope (Ti2-U, Nikon, Japan), and the illumination beam with a central wavelength of 643 nm and a bandwidth of 2 nm is emitted from a supercontinuum fiber laser (SuperK EXU-6, NKT Photonics, Denmark). Left-handed circularly polarized input light incident on the objects of interest is placed on the photonic chip, and the right-handed circularly polarized component of output light passing through the photonic chip is filtered out with imaging conducted onto the detector. We introduce a spherical reference light to interfere with the output field to measure the winding number of topological charge.

Results and Discussions According to the intensity profile in every direction of the back focal plane of the fabricated photonic chip, the optical transfer function of the chip satisfies the form required for second-order differentiation, which means this photonic chip can implement isotropic second-order differentiation. The interference result between reference light and output light represents that there is a second-order topological charge in the expression of optical transfer functions, which leads to isotropic differentiation. The USAF resolution test chart is adopted to demonstrate the performance of this photonic chip. Two peaks at the location of the chart's edge mean second-order differentiation is implemented. Additionally, the edge detection on biological objects indicates that this photonic chip can also be applied to the biological field.

Conclusions We design a two-dimensional second-order topological differential optical chip operating in the transmission mode. The optical chip is composed of all-dielectric one-dimensional photonic crystals. By adjusting the structural parameters of photonic crystals, the optical transfer function required for second-order differential operation can be achieved. When the polarization states of the incident light and the output light are left-handed circularly polarized and right-handed circularly polarized respectively, a second-order topological charge is generated in the optical transfer function to achieve isotropic two-dimensional differential operation. We demonstrate the differential operation effect of the prepared optical chip on the incident light field by employing the USAF resolution test chart and biological sample. This topological differential device characterized by high throughput, high speed, and easy fabrication will have potential applications in optical computing, imaging, and sensing.

Key words physical optics; optical topological differentiation; edge detection; all-dielectric one-dimensional photonic crystals; optical imaging and sensing